DELAMINATIONS IN COMPOSITE PLATES UNDER IMPACT LOADS*

Scott R. Finn and George S. Springer
Stanford University

SUMMARY

A method is presented for calculating the locations, shapes, and sizes of delaminations which occur in a fiber reinforced composite plate subjected to non-penetrating ("low velocity") impact of a solid object. The plate may be simply supported, clamped, or free along its edges. A failure model of the delamination formation was developed. This model was then coupled with a finite element analysis. The model and the finite element analysis were then implemented by a computer code ("IMPACT-ST") which can be used to estimate the damage initiation load and the locations, shapes, and sizes of the delaminations. Tests were performed measuring the geometries of delaminations in graphite-epoxy, graphite-toughened epoxy, and graphite-PEEK plates impacted by a projectile with a spherical tip having masses ranging from 0.355 lbm to 0.963 lbm and velocities from 50 in/sec to 225 in/sec. The data were compared to the results of the model, and good agreements were found between the measured and calculated delamination lengths and widths.

INTRODUCTION

Structures made of fiber reinforced organic matrix composites may become damaged when subjected to impact loads. The damage may manifest itself in the form of fiber breakage, matrix cracking, and delamination. Here, our main focus is on delamination. The reason for this is twofold. First, our interest is damage caused by impact where, in general, delamination is of primary concern. Second, while there are reasonable models for predicting fiber breakage and matrix cracking, there is no accurate method for predicting the locations, shapes, and sizes of delaminations in dynamically loaded composite laminates.

The formation and growth of delaminations in panels subjected to transverse static or dynamic loads have been studied by several investigators. However, the existing methods for predicting the locations, shapes, and sizes of delaminations possess certain limitations. The model of Clark [1] provides only qualitative predictions of the delamination sizes. The models of Bostaph and Elber [2] and Grady, et al [3,4] provide an estimate of the delamination growth but require a priori knowledge of the number and locations of delaminations. In addition, Bostaph and Elber assume that, in cases of

*This work is supported by NASA Langley Research Center under contract number NAS1-18778.

multiple delaminations, all delaminations grow to the same size, while Grady's model applies only to relatively large delaminations. Liu's model [5,6] shows the effect of bending stiffness mismatch between adjacent plies on delamination sizes. The models of Wu and Springer [7] and Gosse, et al [8,9] provide the locations, shapes, and sizes of delaminations. Wu and Springer's model was based on limited experimental data and has since been found not to apply to a broad range of impact conditions. The model of Gosse, still in the development stage, requires a strength parameter for which there is no known test.

It appears that no model exists which would provide with sufficient accuracy the locations, magnitudes, and shapes of delaminations inside composite laminates subjected to the impact of a solid object. Therefore, the first objective of this investigation was to develop a model which can be used to estimate the locations, shapes, and sizes of delaminations inside fiber reinforced composite laminates subjected to transverse non-penetrating ("low velocity") impact. A second objective was to generate data to evaluate the accuracy of the present model as well as any other models which may be forthcoming.

DELAMINATION MODEL

We consider a composite plate made of plies of unidirectional fibers embedded in an organic matrix. The plies may be arranged in groups of neighboring plies which all have the same fiber orientation. Initially, the plies are perfectly bonded. Each edge of the plate may be either clamped, simply supported, or free.

The plate is subjected to transverse impact loading (Figure 1). The objective is to find the "initiation load" (i.e., the load at which delamination first occurs), and the locations, shapes and sizes of the delaminations caused by loads higher than the "initiation load."

Damage Initiation

It has been observed previously [1, 8-17] that delamination is often preceded by transverse matrix cracking. This observation has further been borne out by tests performed during the course of this study. On the basis of this evidence, we postulate that transverse matrix cracking is a necessary precursor to delamination. The load at which transverse matrix cracking first occurs is designated as the "initiation load." This load is estimated by the formula [8, 9]

$$\frac{1}{2}\left(\sigma_{yy} + \sigma_{zz}\right) + \sqrt{\frac{1}{4}\left(\sigma_{yy} - \sigma_{zz}\right)^2 + \sigma_{yz}^2} \quad \begin{matrix} \geq Y & \text{damage} \\ < Y & \text{no damage} \end{matrix} \qquad (1)$$

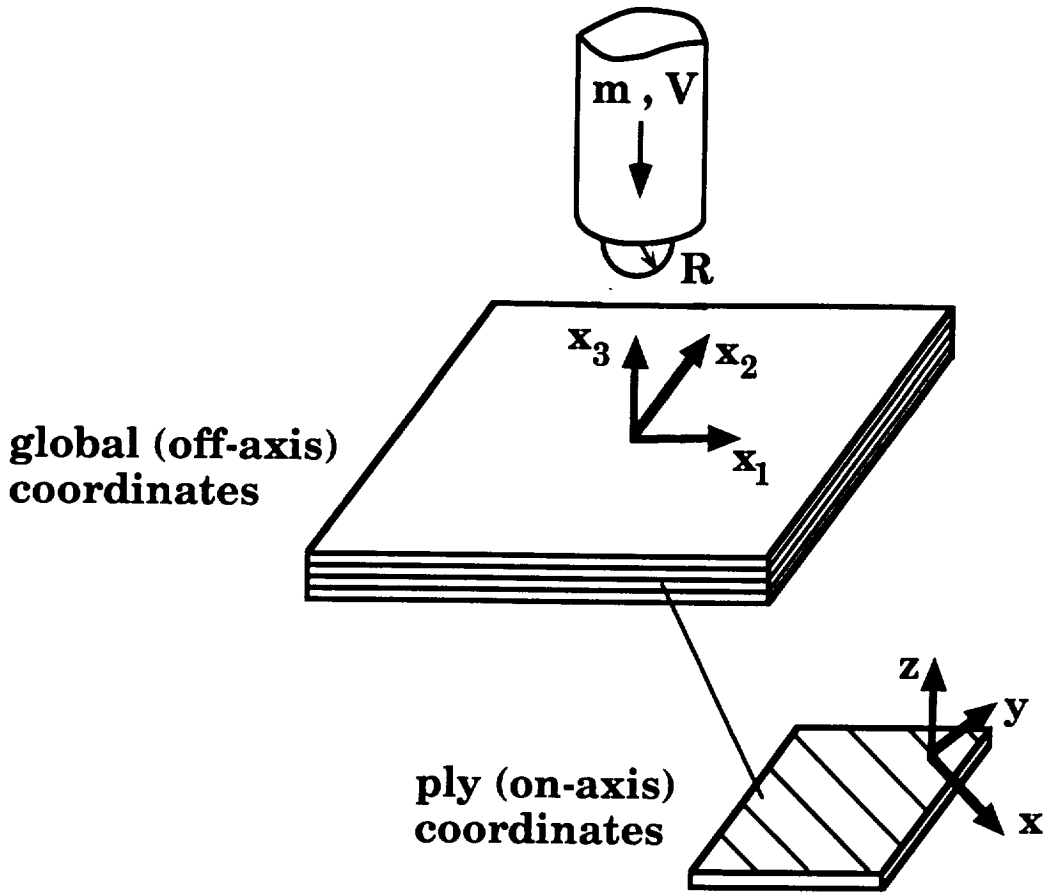

Figure 1 Description of the problem and coordinate systems

where σ denotes stress, and y and z are on-axis coordinates transverse to the fiber direction (Figure 1). Under a given load, matrix cracking occurs when in any given ply group the combination of stresses on the left hand side of this equation equals the ply group's transverse tensile strength Y. This strength is given by [18]

$$Y = Y_o\left(1 + C\frac{\sin(\Delta\theta)}{N^B}\right) \qquad (2)$$

Y_o is the transverse tensile strength of a $[90]_n$ laminate ($n \geq 12$). $\Delta\theta$ is the smaller of the two differences in fiber orientation between the given ply group and the ply groups above and below it. N is the number of individual plies within the ply group. B and C are constants which depend on the material.

Delamination Model

Delamination over a small area dA on an interface occurs when the strain energy available to form the delamination exceeds the energy required to cause delamination [19]. In general terms, this condition can be expressed as

$$\hat{S} \geq G_c dA \tag{3}$$

where $\hat{S}$ is the strain energy available to delaminate dA and G_c is the critical strain energy release rate. The available strain energy is only a portion of the total strain energy inside the plate. The total strain energy is [20]

$$\hat{S}_{total} = \frac{1}{2}\int_V (\sigma_{xx}\varepsilon_{xx} + \sigma_{yy}\varepsilon_{yy} + \sigma_{zz}\varepsilon_{zz} + \sigma_{xy}\gamma_{xy} + \sigma_{xz}\gamma_{xz} + \sigma_{yz}\gamma_{yz})\, dV \tag{4}$$

where ε and γ denote normal and engineering shear strains, respectively. x,y,z are the on-axis (ply) coordinates (Figure 1). V is the volume of the plate.

In order to apply Eq. 3, the relationship between the available and the total strain energies must be known, and the critical strain energy release rate must be specified. There are different avenues by which the available strain energy and the critical strain energy release rate can be established. Here, we propose a model which is built on two basic tenets.

1) Delaminations occur only at interfaces which are adjacent to a ply group in which longitudinal matrix cracking occurs (i.e. the crack is parallel to the fibers [8-10].

2) The matrix crack must open up for a delamination to be produced.

To describe this model we focus our attention on a ply group containing a matrix crack and the two adjacent interfaces (Figure 2). An interface is denoted as either "upper" or "lower", depending on whether it is closer to or further from the load. Each interface may be unrestrained or restrained. An interface is unrestrained either if it coincides with the front or back surface of the plate or if it is delaminated (Figure 3). An interface is restrained when perfect bonding is maintained between the cracked ply group and the adjacent laminate.

Below, the stresses and mechanisms are discussed which, according to our model, cause delaminations in the interfaces adjacent to the cracked ply group. Since our interest is in ply groups with longitudinal matrix cracks, we examine the on-axis stress field in a cracked ply group (Figure 4).

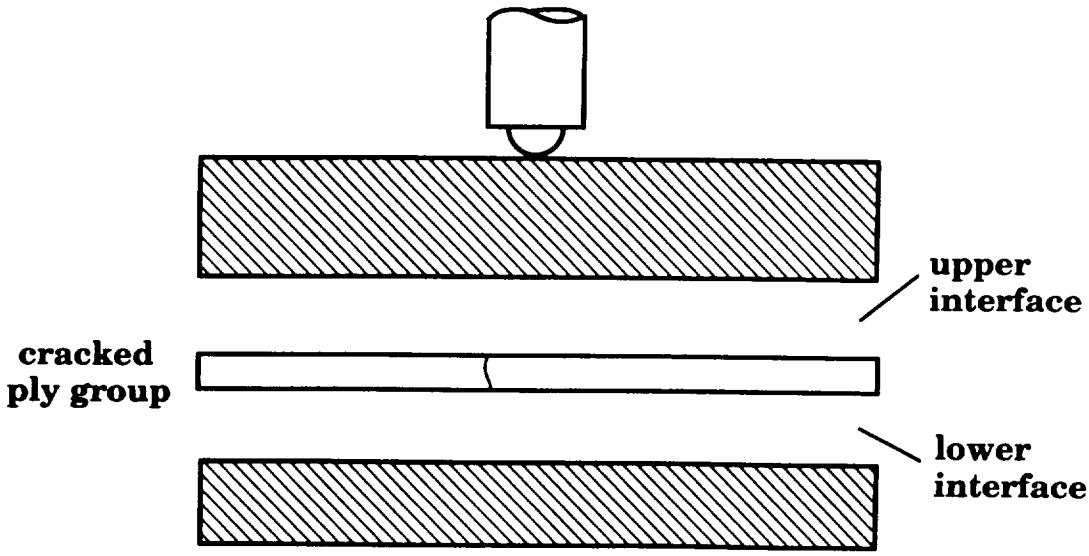

Figure 2 Cracked ply group and corresponding upper and lower interfaces

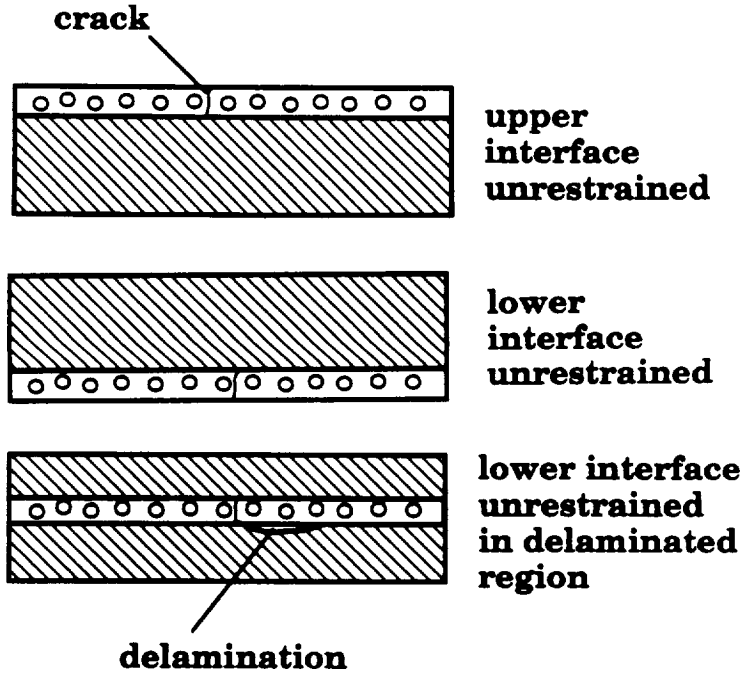

Figure 3 Illustration of an unrestrained interface

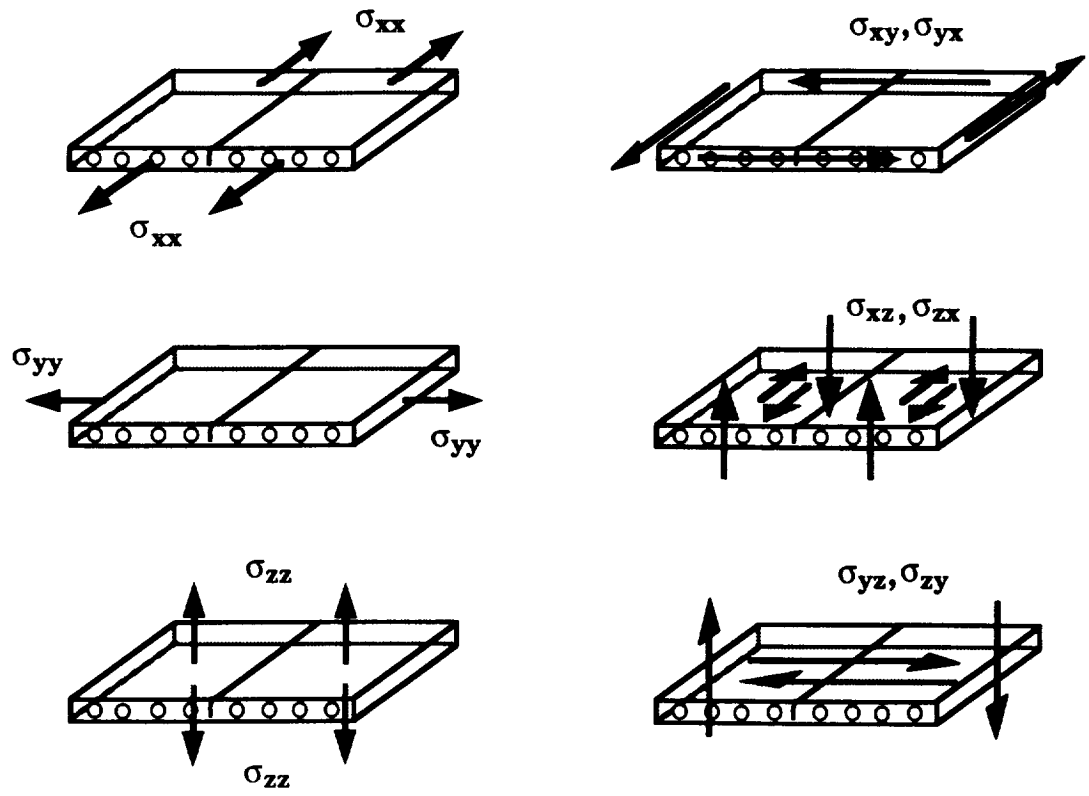

Figure 4 Stress field in a cracked ply group

Bending and Twisting. The applied transverse load may result in bending and twisting of the plate. When a ply group contains a transverse crack (and this ply group is unrestrained) the curvature of the cracked ply group will be different than that of the adjacent laminate. This difference of curvature causes a separation (delamination) between the cracked ply group and its neighboring ply groups.

First, we consider the case when the plate has a concave bend with respect to the applied load, and the lower interface of the cracked ply group is unrestrained (Figure 5). This bending introduces curvatures in the directions normal and parallel to the fibers. In the former case, the crack may open resulting in a difference in curvature between the cracked ply group and the laminate. As a consequence of this, delamination occurs along the upper interface, as depicted in Figure 5 (left). The stress in the cracked ply group associated with the bending just described is the in-plane normal tensile stress σ_{yy}^{+}. This stress must be included when calculating the strain energy available to delaminate the upper interface. Note that if the lower interface is restrained, the crack is not free to open and no delamination is produced.

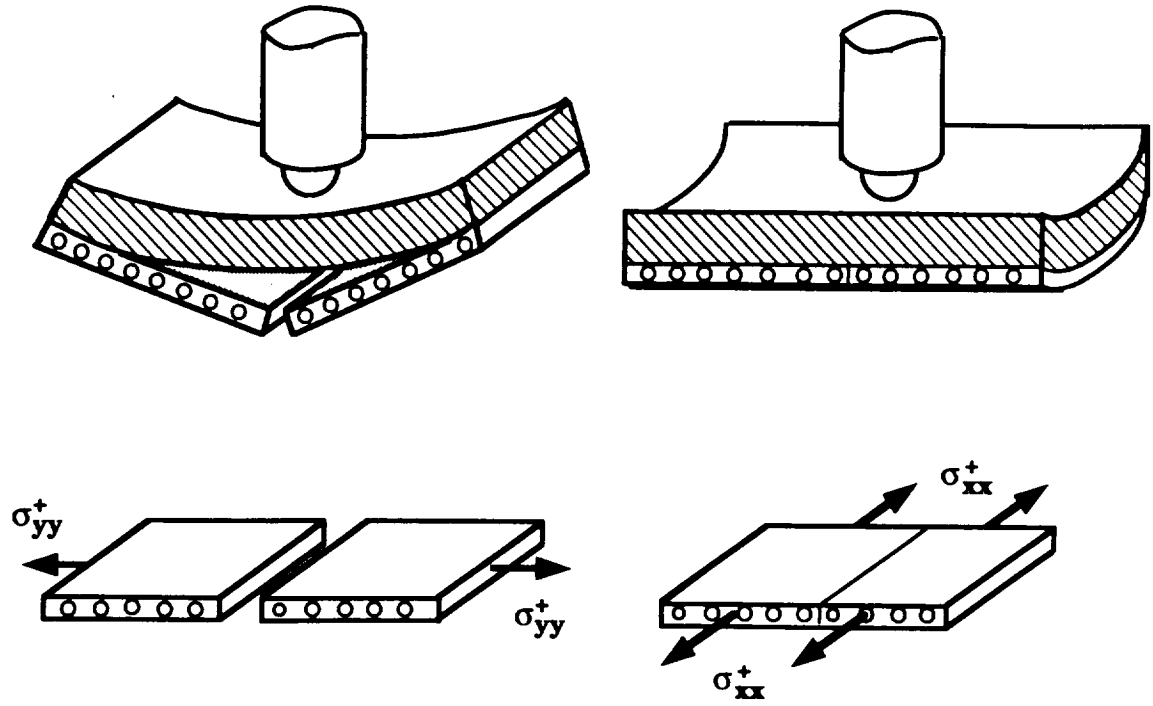

Figure 5 Bending of a plate containing a cracked ply group with its lower interface unrestrained; left: curvature in the direction normal to the fibers of the cracked ply group, right: curvature in the direction parallel to the fibers of the cracked ply group

The above scenario applies when the curvature is concave with respect to the applied load. There might be a slight convex curvature when the plate rebounds. Delamination growth resulting from this condition is neglected.

Bending may also cause a change in curvature along the fiber direction of the cracked ply group (Figure 5, right). Neglecting Poisson effects, this bending does not tend to open the matrix crack and thus, according to our model, does not contribute to delamination. In the cracked ply group, this type of bending is associated with a normal tensile stress in the fiber direction σ^+_{xx}. Since bending in the fiber direction does not play a role in delamination, σ^+_{xx} is not included in the expression for the available strain energy.

The aforementioned discussion applies when the lower interface of the cracked ply group is unrestrained. When the upper interface of the cracked ply group is unrestrained (Figure 6), the cracked ply group is in compression, the crack does not open and no delamination occurs. Hence, the associated transverse compressive stresses σ^-_{yy} and σ^-_{xx} need not be considered when calculating the available strain energy.

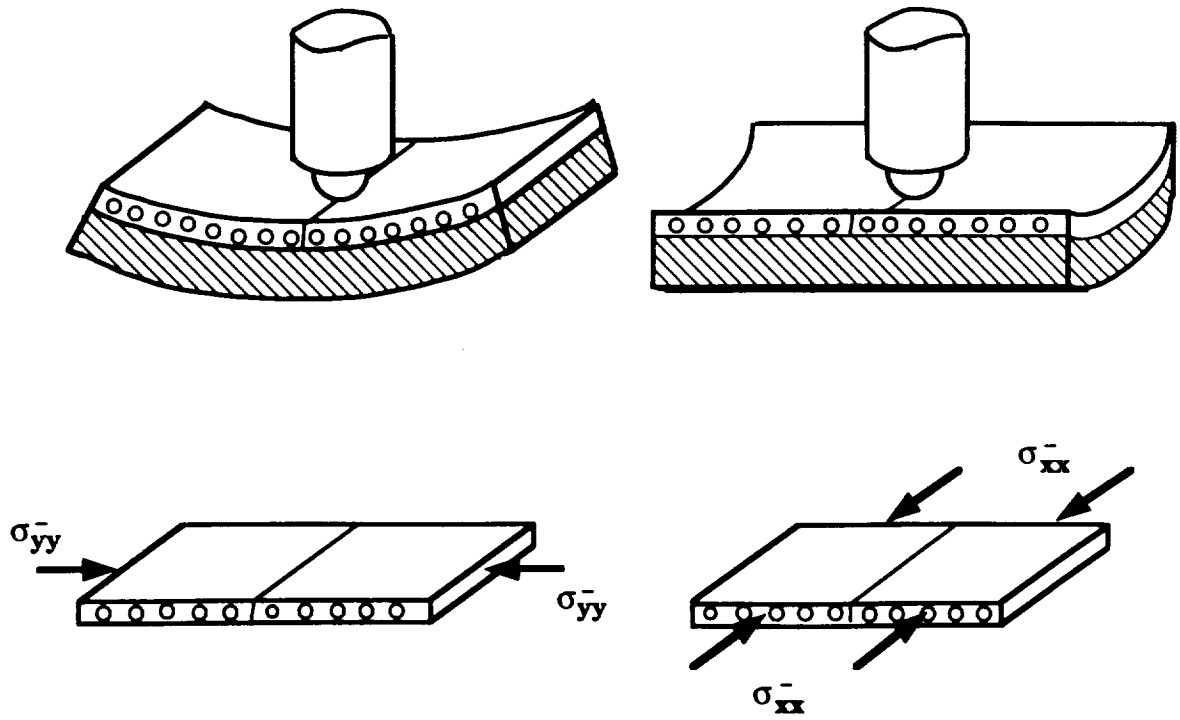

Figure 6 Bending of a plate containing a cracked ply group with its upper interface unrestrained; left: curvature in the direction normal to the fibers of the cracked ply group, right: curvature in the direction parallel to the fibers of the cracked ply group

The transverse load may also cause a twisting of the plate (Figure 7). If the lower interface is unrestrained, the crack may open, resulting in a mismatch in curvature between the cracked ply group and the laminate above it. This mismatch in curvature causes a delamination to form along the upper interface. The converse situation exists if the upper interface is unrestrained. The twisting motion just described is associated with an in-plane shear stress σ_{xy} in the cracked ply group. This stress must be considered when calculating the strain energy available to create a delamination at either the upper or lower interface. If both interfaces are restrained, the crack is not free to open and no delamination is formed.

Transverse Shear. The applied transverse load causes shearing of the plate. Shear may cause two adjacent ply groups to slide relative to one another (Figure 8). This motion does not affect the matrix crack which means that, according to our model, it does not contribute to delamination. The deformation shown in Figure 8 is associated with either or both of the transverse shear stresses σ_{zx} and σ_{zy}. Since the crack does not open, this mechanism would not require that σ_{zx} and σ_{zy} be included in the calculation of the available strain energy.

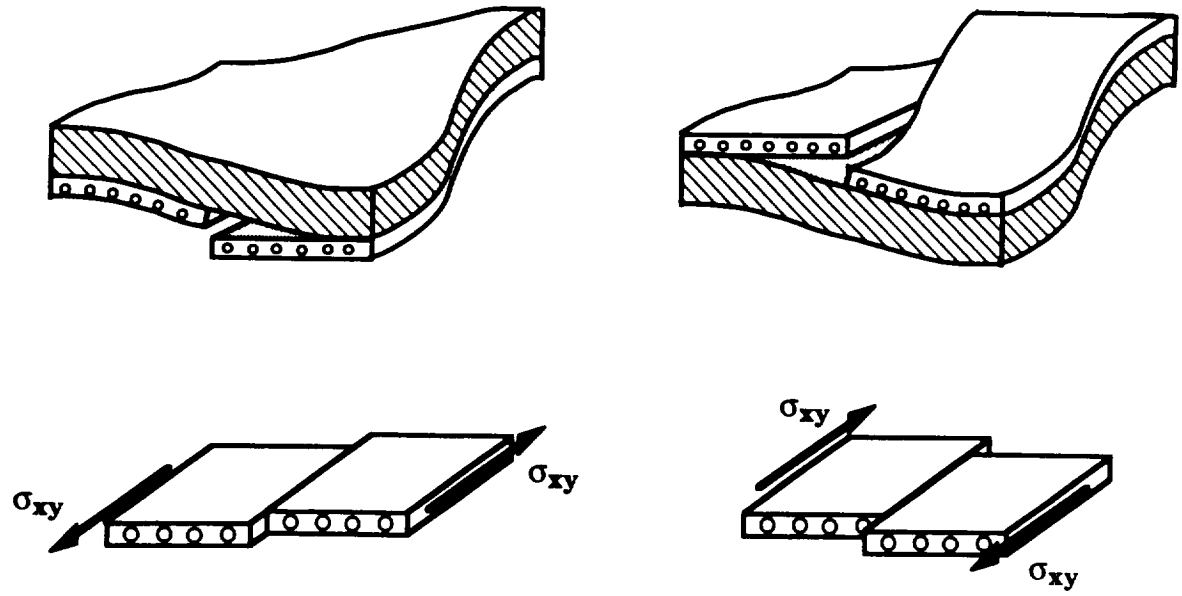

Figure 7 Twisting of a plate containing a cracked ply group; left: with lower interface unrestrained, right: with upper interface unrestrained

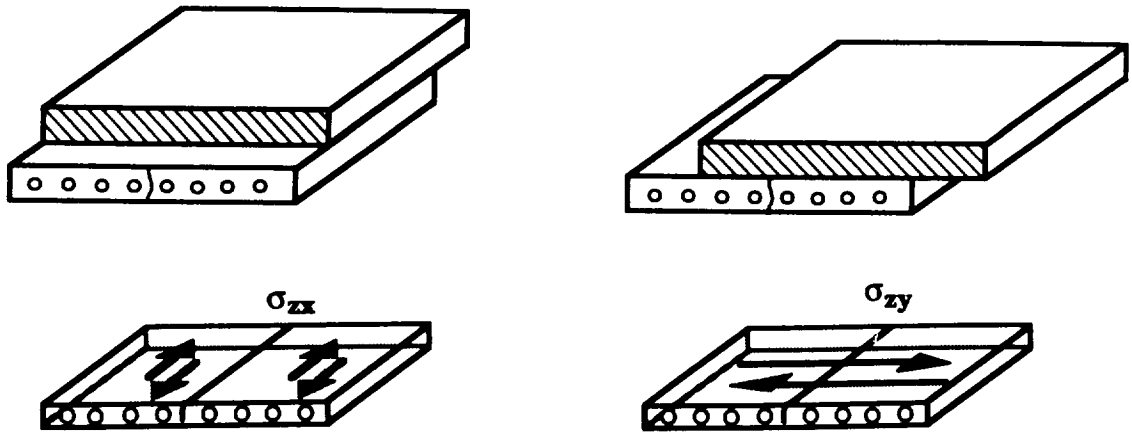

Figure 8 Interlaminar shearing of a cracked ply group; left: parallel to the fiber direction of the cracked ply group, right: normal to the fiber direction of the cracked ply group

The transverse shear introduced by the applied load also introduces local curving in the directions normal and parallel to the fibers of the cracked ply group (Figure 9). In the presence of a cracked ply group the shear introducing a curvature in the direction normal to the fibers creates a local mismatch in curvature between the cracked ply group and the adjacent ply groups (Figure 9, left). This local mismatch in curvature results in delaminations along both the upper and lower interfaces. The delamination starts at the crack and grows in the direction away from the load at the lower interface and towards the load at the upper interface. Since the inital cracks are generally located near the load, the delamination at the upper interface is smaller than that at the lower interface and is neglected in our model. This type of shearing is associated with the transverse shear stress σ_{yz} in the cracked ply, which therefore must be included in the calculation of the strain energy available to delaminate the lower interface.

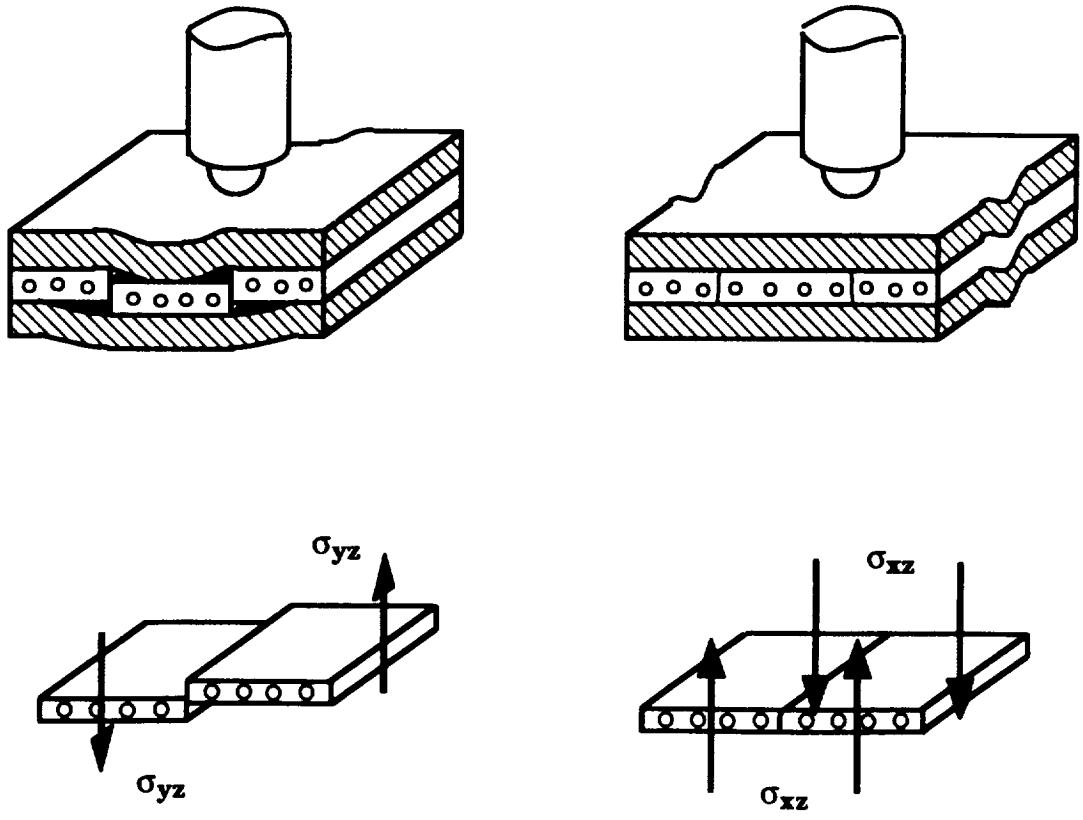

Figure 9 Shearing of a ply containing a cracked ply group; left: shear-induced local curvature normal to the fibers of the cracked ply group, right: shear-induced local curvature parallel to the fibers of the cracked ply group

Shearing may also cause a local curvature along the fiber direction of the cracked ply (Figure 9, right). This deformation does not open the matrix crack, and thus does not lead to delamination. Hence, the transverse shear stress σ_{xz}, which is associated with this type of deformation, need not be included in the calculation of the available strain energy.

Thickness Changes. Inside the plate, forces (with corresponding stresses σ_{zz}) may stretch or compress the ply groups in the thickness direction (Figure 10). Neglecting Poisson effects, this deformation does not open the matrix crack and, thus, has no affect on delamination. Since delamination does not occur, σ_{zz} is not considered when calculating the available strain energy.

Available Strain Energy. According to our model, delamination is mostly caused by differences in curvature between a cracked ply group and the adjacent laminate. Hence, when calculating the available strain energy, we include only those terms in the strain energy which are directly related to the change in curvature. Referring to the previous discussion, we note that these terms are the in-plane stresses σ^{+}_{yy} and σ_{xy} and the transverse shear stress σ_{yz}. Further, we only take into account the available strain energy of the cracked ply group. Thus, to establish the expression for the strain energy available to form a delamination, we need to consider only an interface bounded by a "top" and "bottom" ply group. The terms "top" and "bottom" refer to the ply groups which are closer to and further from the load, respectively.

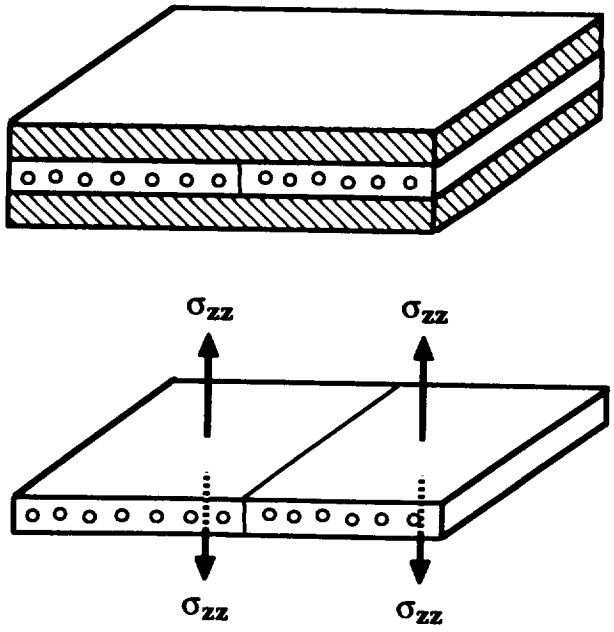

Figure 10 Normal stresses causing changes in the thickness of a cracked ply group

Then, the energy available for delamination of the interface may be supplied by both the top and bottom ply groups

$$\hat{S} = \hat{S}_t + \hat{S}_b \qquad (5)$$

where $\hat{S}_t$ and $\hat{S}_b$ are the strain energies contributing to the delamination from the top and bottom cracked ply group, respectively.

We now summarize our previous discussion on the formation of delaminations.

a) A ply group must be cracked to cause delamination along an adjacent interface.

b) A top ply group (i.e., the cracked ply group above the interface) contributes to the strain energy available to create delamination only through the stresses σ_{xy} and σ_{yz} (Figure 11). In order for the stress σ_{xy} to contribute to the delamination, the ply group's upper interface must be unrestrained.

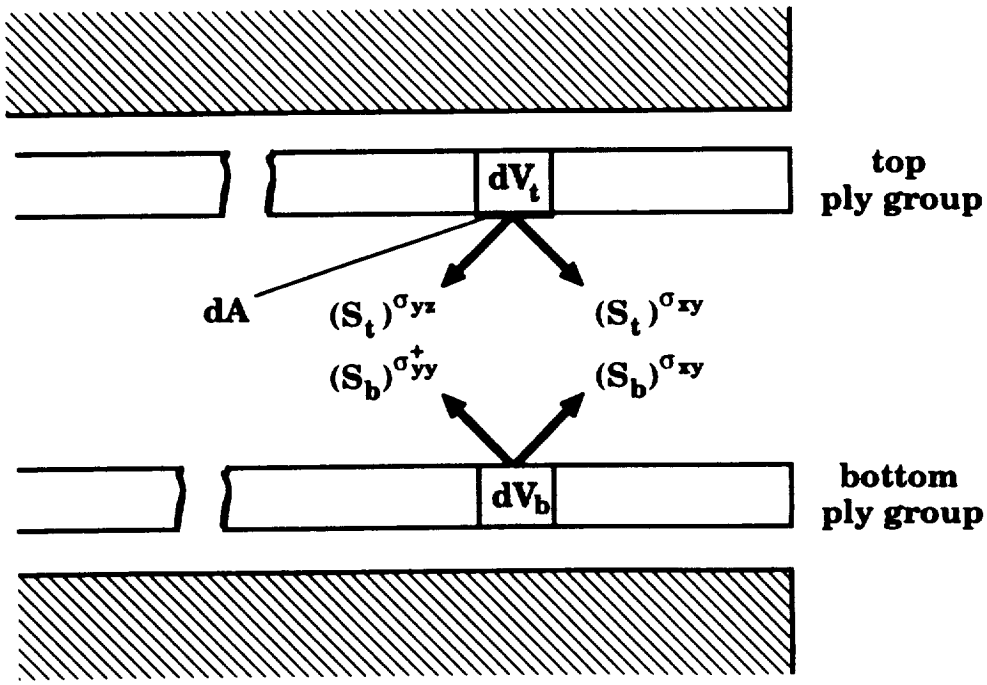

Figure 11 Stresses from the top and bottom cracked ply groups contributing to the strain energy available to form a delamination

c) A bottom ply group (i.e., the cracked ply group below the interface) contributes to the available strain energy only through the stresses σ_{yy}^{+} and σ_{xy} (Figure 11). For either of these stresses to contribute to the delamination, the ply group's lower interface must be unrestrained.

In terms of the strain energy density S, the condition for delamination is

$$S_t dV_t + S_b dV_b \geq G_c dA \tag{6}$$

where dV_t and dV_b are volume elements in the top and bottom ply groups corresponding to the surface area dA (Figure 11). The available strain energy densities (energy per unit volume) are

$$S_t = \frac{1}{2}\left(\sigma_{yz}\gamma_{yz} + \Omega\sigma_{xy}\gamma_{xy}\right) \tag{7}$$

$$S_b = \frac{1}{2}\Omega\left(\sigma_{yy}^{+}\varepsilon_{yy} + \sigma_{xy}\gamma_{xy}\right) \tag{8}$$

Ω equals 1 if the ply group's "other" interface is unrestrained and 0 if it is restrained. Recall that x, y, and z are ply coordinates (Figure 1) and are different for the top and bottom ply groups.

In our model, delaminations are primarily caused by curvature changes in the cracked ply. These curvature changes result in a separation of the plies in the direction normal to the interface rather than in sliding between the plies. The critical strain energy release rate G_c corresponding to this type of separation is the mode I critical strain energy release rate G_{Ic}. Thus, the expression for predicting delamination at a point on an interface (Eq. 3) is written as

$$S_t dV_t + S_b dV_b \geq G_{Ic} dA \tag{9}$$

where S_t and S_b are given by Eqs (7) and (8). It is emphasized that S_t and S_b are taken into account only when the corresponding top or bottom ply group is cracked.

Delamination Locations, Shapes, and Sizes

The delamination model described above is implemented in the following manner. First, the strain energy available per unit area S_a is calculated at every point of the interface by the expression

$$S_a = \int_{h_t} S_t dz + \int_{h_b} S_b dz \qquad (10)$$

where h_t and h_b are the thicknesses of the top and bottom cracked ply groups, respectively. The point is identified where this available strain energy is the highest (Figure 12a). At this point, a small rectangular element of area A_1 is considered (Figure 12b), and the available strain energy is compared to the critical strain energy necessary to delaminate the area. If the available strain energy is greater than the necessary strain energy, it is assumed that the interface delaminates over this area. Mathematically, this condition is expressed as

$$\int_{A_1}\left[\int_{h_t} S_t dz + \int_{h_b} S_b dz\right]dA \quad \begin{array}{ll} \geq G_{Ic}A_1 & \text{delamination} \\ < G_{Ic}A_1 & \text{no delamination} \end{array} \qquad (11)$$

Once the elemental area A_1 is found to be delaminated, the available strain energy per unit area S_a is calculated on the interface outside the delaminated area A_1 and again the point is identified where S_a is highest (Figure 12c). Then, a small rectangular element A_2 about this point is added to the area previously found to be delaminated (Figure 12d). In practice, area A_2 always adjoins area A_1. The delamination is taken to extend into area A_2 if the available strain energy is greater than the strain energy necessary for delamination

$$\int_{A_1+A_2}\left[\int_{h_t} S_t dz + \int_{h_b} S_b dz\right]dA \quad \begin{array}{ll} \geq G_{Ic}(A_1 + A_2) & \text{delamination} \\ < G_{Ic}(A_1 + A_2) & \text{no delamination} \end{array} \qquad (12)$$

The above procedure is then repeated. For the nth repetition (Figures 12e,f), we have

$$\int_{A_{tot}}\left[\int_{h_t} S_t dz + \int_{h_b} S_b dz\right]dA \quad \begin{array}{ll} \geq G_{Ic}A_{tot} & \text{delamination} \\ < G_{Ic}A_{tot} & \text{no delamination} \end{array} \qquad (13)$$

where A_{tot} is

$$A_{tot} = (A_1 + A_2 + \ldots + A_n) \qquad (14)$$

At each time step, this procedure is repeated until no further delamination is predicted on the interface under consideration. Every

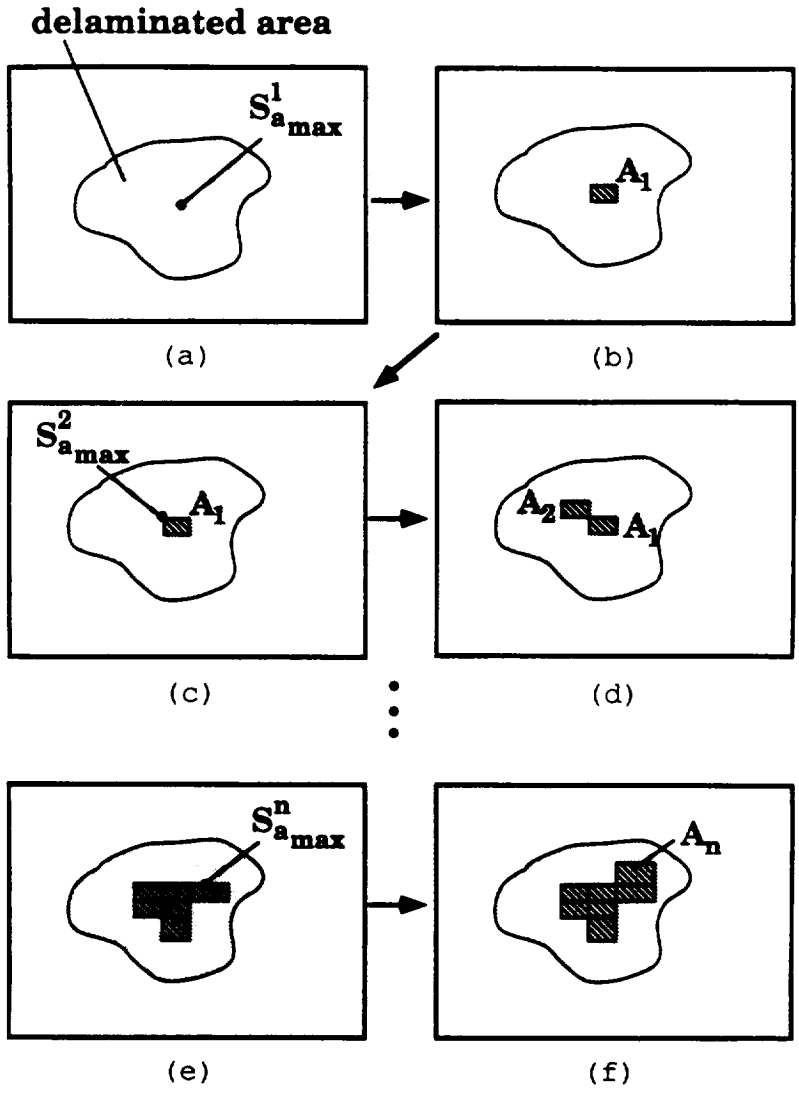

Figure 12 Steps in calculating the delamination shapes and sizes

interface inside the plate is inspected in this manner, resulting in the shapes and sizes of the delaminations along every interface. These calculations require, of course, a knowledge of the stress and strain distributions in the plate. Procedures for calculating these parameters as well as the characteristics of the delaminations are presented in the next two sections.

METHOD OF SOLUTION

Contact Force

To perform the analysis, the contact force between the plate and the impactor must also be specified. The impactor is taken to be an elastic solid with a hemispherical contact surface. To determine the contact force between the impactor and the plate during loading, the Hertzian contact model [20] is used. According to this model, the contact force F during loading is related to the indentation depth α by the equation

$$F = \kappa\alpha^{1.5} \tag{15}$$

where κ is a constant that depends on the nose radius R, the material of the impactor, and the material of the plate. For layered composite materials a suitable expression for κ is [21]

$$\kappa = \frac{4}{3}\sqrt{R}\,\frac{1}{\left[\left(1 - \nu_s^2\right)/E_s + 1/E_{yy}\right]} \tag{16}$$

where ν_s and E_s are the Poisson's ratio and Young's modulus of the impactor, and E_{yy} is the Young's modulus of the top ply in the direction normal to the fibers.

Permanent deformation often occurs below the contact area during loading, and, therefore, different relations are needed for unloading and loading. For unloading, the following expression was proposed by Yang and Sun [21]

$$F = F_m\left[\frac{\alpha - \alpha_o}{\alpha_m - \alpha_o}\right]^{2.5} \tag{17}$$

where F_m is the maximum contact force and α_m is the maximum indentation during loading. α_o is the permanent deformation given by

$$\alpha_o = 0 \qquad \alpha_m < \alpha_{cr} \tag{18}$$

$$\alpha_o = \alpha_m \left[1 - \left(\frac{\alpha_{cr}}{\alpha_m} \right)^{0.4} \right] \qquad \alpha_m \geq \alpha_{cr} \qquad (19)$$

In these equations, α_{cr} is a material constant, which for graphite/epoxy materials has been found to be 0.00316 inch [21].

Because neither the impactor nor the plate are rigid, the load is distributed over a small area around a central point, this point being directly beneath the center of the impactor. According to the Hertzian model, the pressure distribution about this central point can be approximated by [20]

$$p(r) = \frac{3F}{2\pi a^3} \sqrt{a^2 - r^2} \qquad (20)$$

where r is the distance from the central point, and a is the radius of the contact region given by

$$a = \sqrt[3]{\frac{(F)(R)^{1.5}}{\kappa}} \qquad (21)$$

Stress Analysis

The stress analysis can best be effected by finite element methods. Different finite element approaches have been proposed in the past which can be applied to the present problem. In this study, for convenience, we adopt the method of Wu and Springer [7], since the IMPACT computer code based on this method has proven to be useful in calculating transient stresses in composite plates subjected to impact loading. Details of the finite element formulation is described in detail elsewhere [7, 22] and is not repeated here . The two main features of the formulation are the use of three-dimensional brick elements and incompatible modes. The brick elements may contain more than one ply group per element so that plies with different fiber orientations can be inside the same element. Incompatible modes were included in the element shape functions to improve the bending response of the elements [23, 24]. The analysis provides all six components of the stresses in plates whose edges amy be clamped, simply supported, or free.

Generally, the calculations are performed with an element containing more than one ply group. The element stiffness is obtained by averaging or "smearing" the stiffnesses of the individual ply groups. This is accomplished for an element with n ply groups by calculating the element's elasticity tensor in terms of the elasticity tensors of the individual ply groups

$$\left(E_{ijkl}\right)_{el} = \frac{1}{h_{el}}\left[h_1\left(E_{ijkl}\right)_1 + h_2\left(E_{ijkl}\right)_2 + \ldots + h_n\left(E_{ijkl}\right)_n\right] \quad (22)$$

where h_{el} is the thickness of the element containing n ply groups of thickness h_m (m=1,2,...,n). The displacements and corresponding strains in each element are calculated with the average stiffness of the element. However, the stresses in a ply group are calculated from the strains using the elasticity matrix of the individual ply group.

The finite element calculations result in the displacements in the plate as functions of position and time. From these, the stresses and strains are calculated as functions of time at every point inside each element. The numerical calculations can readily be performed by the IMPACT code. However, in its original form, the code was only for dynamic (impact) loads applied to plates supported along all four edges. To extend the applicability of the code, it was modified to include a) statically applied loads, and b) plates with up to three free edges. The resulting code is designated as IMPACT-ST. In addition to the displacements, stresses, and strains this code also includes an algorithm to calculate the delamination locations, shapes, and sizes (see below). Furthermore, in the original IMPACT code, calculations are always performed for the entire plate. In the IMPACT-ST code calculations may be performed only for a quarter of the plate, if proper symmetry exists. This increases the calculation speed by a factor of 15 to 20.

Delamination

The locations, shapes and sizes of delaminations are determined by the use of Eqs. 7-9, 13, and 14. These equations can be written in the form

$$\frac{1}{2}\left[\int_{h_t}\int_{A_1+A_2+\ldots+A_n}\left(\sigma_{yz}\gamma_{yz} + \Omega\sigma_{xy}\gamma_{xy}\right)dAdz + \right.$$

$$\left.\int_{h_b}\int_{A_1+A_2+\ldots+A_n}\Omega\left(\sigma^{+}_{yy}\varepsilon_{yy} + \sigma_{xy}\gamma_{xy}\right)dAdz\right] \quad (23)$$

$$\lesseqgtr \; G_{Ic}\left(A_1 + A_2 + \ldots + A_n\right)$$

When integrating over dA, the areas A_1, A_2, ..., A_n are taken to coincide with the area of an element in the x_1-x_2 plane of the plate. The stresses and strains in this area are assumed to be constant with a value corresponding to that in the center of the area. When integrating across the thickness (z direction) of the ply group, the stresses and strains are taken to be constant across each ply inside the ply group. The stress and strain values used in the calculations are those which

correspond to the stresses and strains at the center of the ply.

Once the stresses and strains are known, Eq. 23 can be applied to establish the locations, shapes, and sizes of the delaminations in the plate. In using this equation, the strain energies in a cracked ply group must be apportioned to its upper and lower adjacent interfaces. To perform the calculations, a post-processor DELAM-TRL was written. For specified stress and strain distributions in the plate, this post-processor provides the geometry (shape and size) of the delamination at every interface in the plate.

The DELAM-TRL code can be incorporated into any appropriate stress analysis code. However, in the calculations care must be exercised to account for the changes in plate response as delaminations develop and grow inside the plate. We combined the DELAM-TRL code with the IMPACT-ST code, accounting for the effects of the delaminations as described below.

As delaminations develop and grow inside a plate, the stress field and hence the available strain energy change under a given applied load. Delaminations reduce the overall stiffness of the plate, generally resulting in deflections which are higher than those which would occur in an undamaged plate. However, during impact loading, delamination is accompanied by a decrease in the applied load [25]. This decrease in the applied load may offset the change in the strain energy caused by the increased displacement due to delamination. Utilizing this observation for impact loading, the available strain energies in the cracked ply groups are taken to be the same as in the corresponding uncracked ply groups.

EXPERIMENTS

Tests were performed measuring the locations, shapes, and sizes of delaminations formed in composite plates subjected to transverse impact loads. The plates were made of unidirectional tape of graphite/epoxy (ICI Fiberite T300/976), graphite/toughened epoxy (ICI Fiberite IM7/977-2), or graphite/PEEK (ICI Fiberite APC-2). The plates were manufactured according to the procedures described in reference 26. After manufacture, each plate was inspected by an ultrasonic technique (C-scan) to establish that they were undamaged.

The plates were three inches wide and six inches long. The plates were inserted in specially built aluminum fixtures which clamped the two opposite, narrow edges of the plate (Figure 13). The two longitudinal edges of the plate were unsupported (free edges).

The force was provided by a projectile (impactor) propelled by pressurized air from a gun (Figure 14). The impactor consisted of a 3 inch tall, 2 1/2 inch wide, and 2 1/2 inch long teflon block with a steel hemisphere attached to the center of one of the ends. The mass of the impactor could be changed by attaching weights to the teflon block.

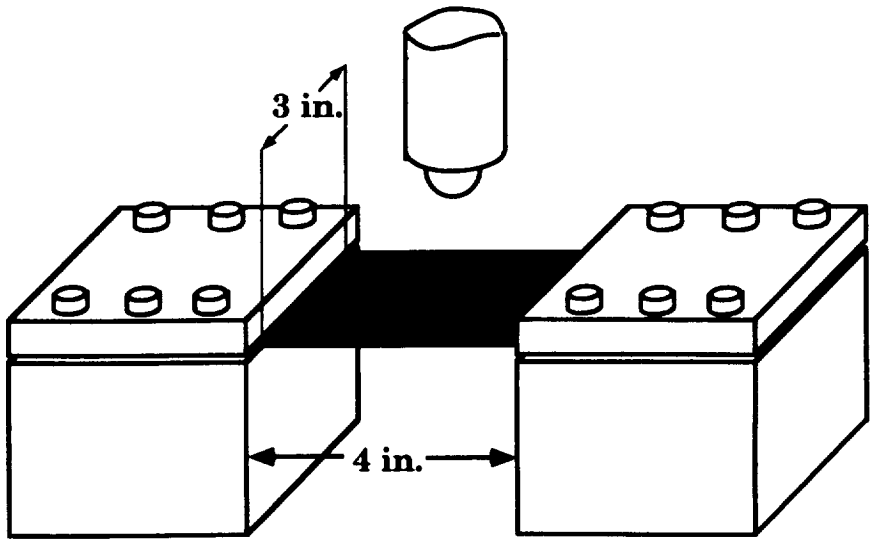

Figure 13 Test fixture used in impact tests

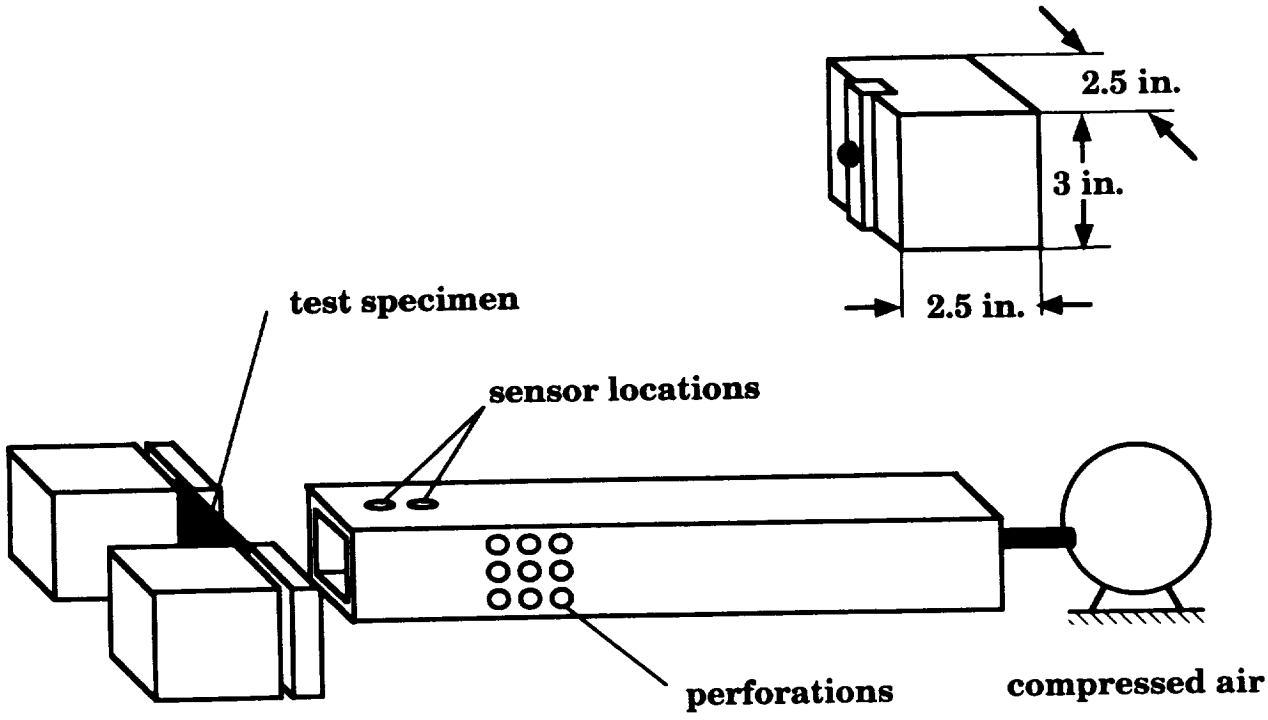

Figure 14 Impact test apparatus and the impactor

The fixture containing the plate was mounted at the exit of the gun so that the impactor hit the center of the plate. The impact velocity could be adjusted by changing the pressure of the air in the gun and the mass of the impactor. The impact velocity was measured by optical sensors placed near the exit of the gun. The barrel was perforated near the exit providing a quick release of the pressure. This facilitated rebounding of the impactor and prevented the impactor from hitting the plate more than once. After impact, each plate was inspected by C-scan and by X-ray. To make the damaged areas visible by X-ray, a dye penetrant (di-iodobutane) was applied to the edges of the plate as well as to any cracks on the surface of the plate. The pulse-echo C-scan technique provided the shape and dimensions of the delamination shape and dimensions at each ply group interface. The X-ray technique yielded the outermost periphery of all the delaminations inside the plate as well as the locations of the matrix cracks.

RESULTS

In this section the test results obtained by impacting Fiberite T300/976 graphite-epoxy, Fiberite IM7/977-2 graphite-toughened epoxy, and ICI APC-2 graphite-PEEK plates are presented. The plates were impacted by an impactor with a nose radius of R = 0.25 or 0.125 in. The impact velocity ranged from 50 in/sec to 225 in/sec, and the mass of the impactor from 0.355 lbm to 0.963 lbm. These velocities and masses resulted im impact energies from 1.15 lbf-in to 63.1 lbf-in. The test conditions are summarized in Table 1.

After impact each plate was inspected by X-ray and by C-scan. The sizes and shapes of the delaminations were deduced by these techniques. The data for all 106 plates tested are not given here but can be found in reference 26. Only a representative set of data is presented in Figure 15. In this figure the calculated delamination lengths and widths are shown as solid lines. Although all the data are not included in this paper in such detail, a summary of the data is presented in Figure 16. In this figure the measured delamination lengths and widths are plotted against the delamination lengths and widths calculated by the present model.

The results in Figures 15 and 16 show that the measured and calculated delamination lengths and widths agree well. In fact, the model not only provides the overall dimensions of the delaminations but also describes reasonably well the shapes of the delaminations. To illustrate this, three typical results are shown here (Figure 17). Similar agreements were found between the measured and calculated delamination shapes for the other plates tested.

The aforementioned comparisons (Figures 15-17) between the data and the results of the model lend confidence to the model.

Table 1. Summary of conditions of impact tests

Fiberite T300/976 (impactor nose radius R = 0.25 in)

Layup	Impactor mass, m (lbm)	Impactor Velocity, V (in/sec)
$[0_2/90_6]_S$	0.355	110, 123, 133, 135, 166, 167, 167, 167, 170, 178
$[0_3/90_5]_S$	0.355	133, 173, 191
$[0_4/90_4]_S$	0.355	46, 54, 89, 92, 105, 108, 109, 110, 111, 111, 112, 119, 121, 128, 135, 141, 141, 142, 152, 156, 161, 162
	0.395	129
	0.432	121
	0.472	122
	0.511	116
	0.704	148, 148, 158
	0.894	169, 208
$[0_5/90_3]_S$	0.355	97, 100, 107, 138
$[0_6/90_2]_S$	0.355	68, 71, 85, 101, 102, 109
$[0_4/20_4]_S$	0.355	92, 98, 128, 135, 147, 154, 164
$[0_4/40_4]_S$	0.355	129, 157
$[0_4/60_4]_S$	0.355	163
$[0_4/80_4]_S$	0.355	162
$[0_2/90_2]_S$	0.355	147, 163
$[0_3/90_3]_S$	0.355	147
$[0_5/90_5]_S$	0.355	133

Table 1. Summary of conditions of impact tests (cont.)

Fiberite IM7/977-2 (impactor nose radius R = 0.25 in)

Layup	Impactor mass, m (lbm)	Impactor Velocity, V (in/sec)
$[0_4/90_4]_S$	0.355	129, 136, 158, 179
	0.511	156
	0.704	151, 207
	0.963	155, 162, 178

ICI APC-2 (impactor nose radius R = 0.25 in)

Layup	Impactor mass, m (lbm)	Impactor Velocity, V (in/sec)
$[0_4/90_4]_S$	0.355	125, 129, 142, 154, 158, 172, 182
	0.704	155
	0.963	203, 228

ICI APC-2 (impactor nose radius R = 0.125 in)

Layup	Impactor mass, m (lbm)	Impactor Velocity, V (in/sec)
$[0_4/90_4]_S$	0.355	141, 146, 150, 161, 169, 170, 170, 171, 171, 172, 173, 176, 177, 183
	0.432	178, 179
	0.511	183

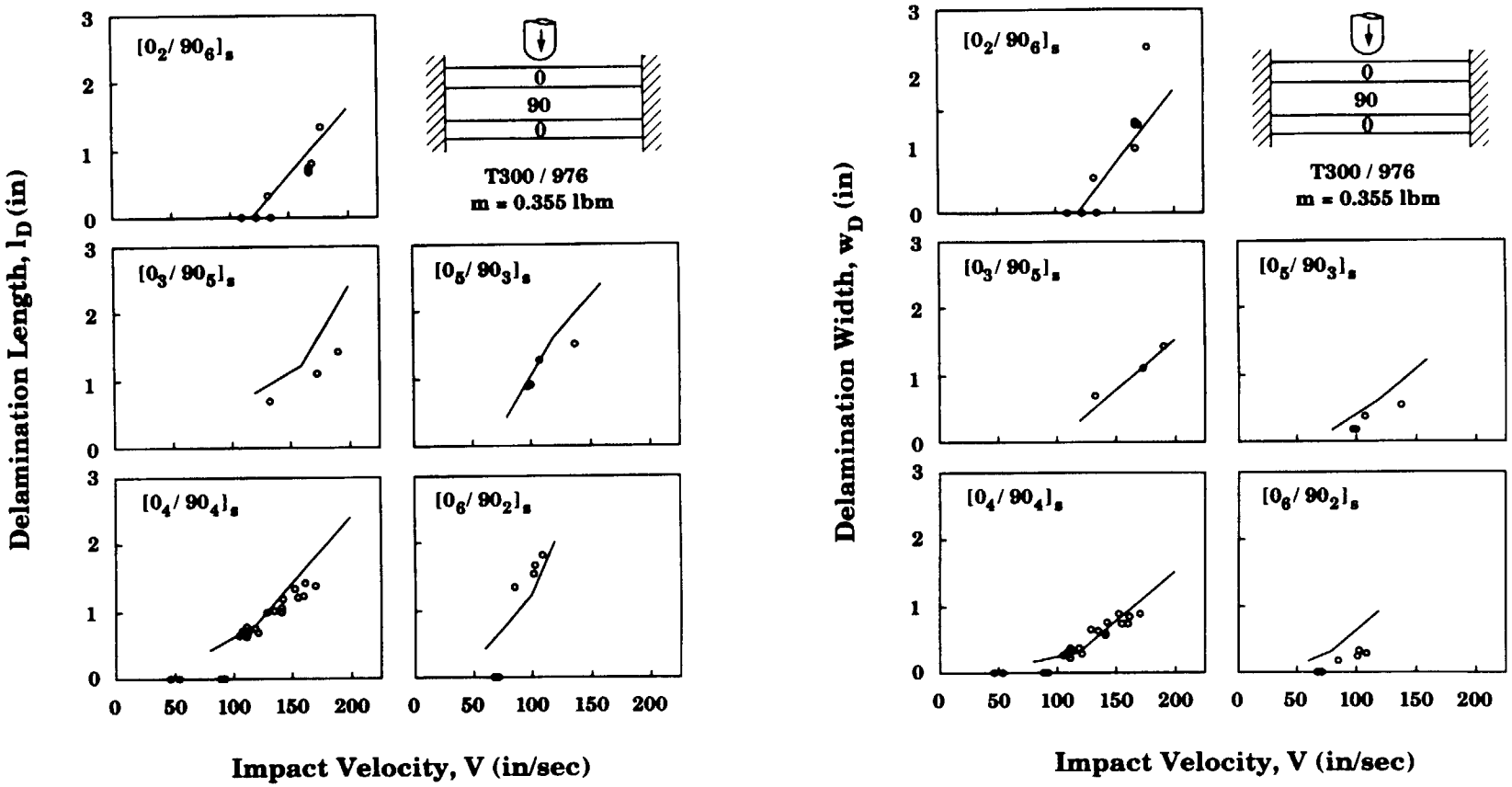

Figure 15 Delamination lengths and widths versus impact velocity for one test set

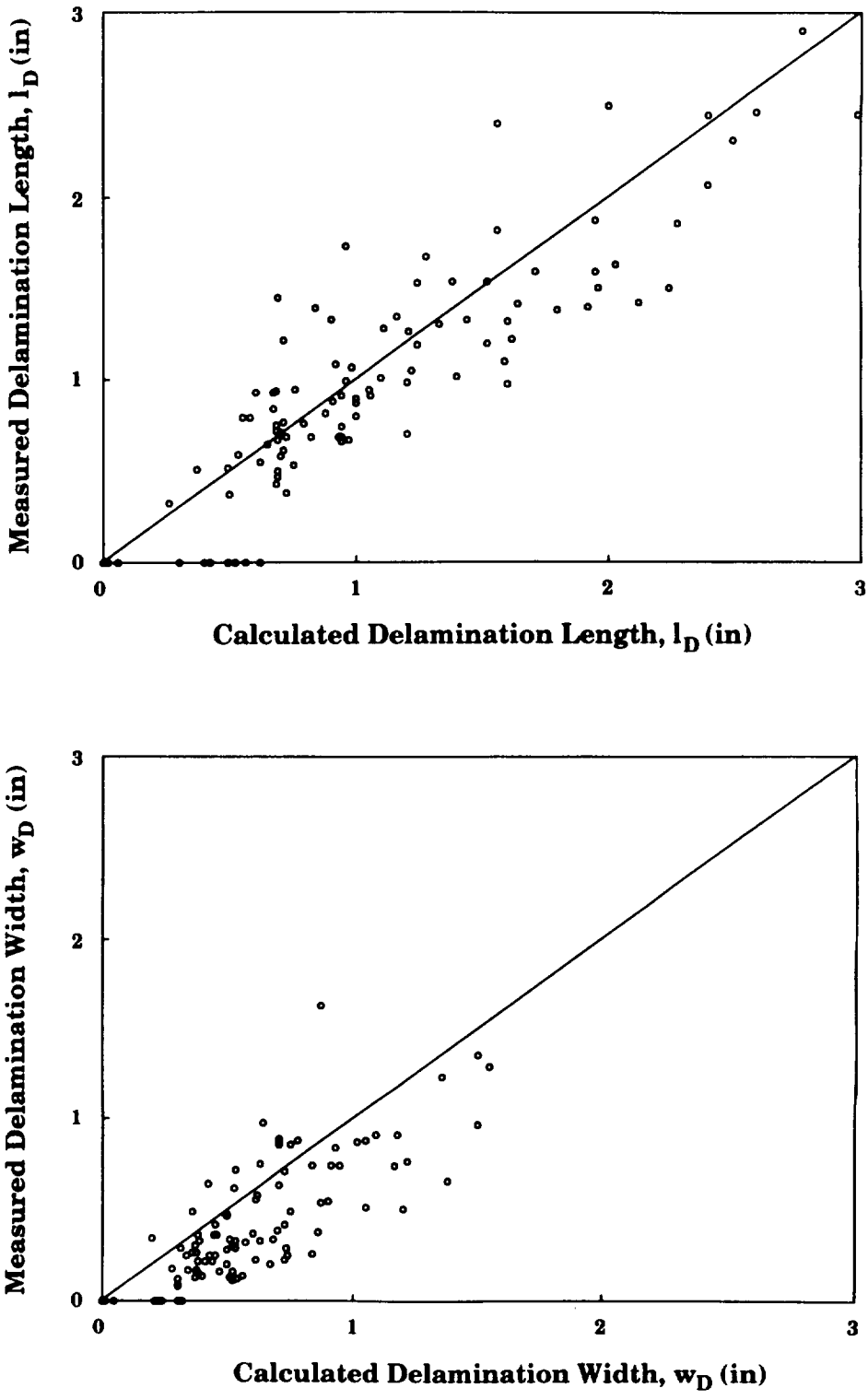

Figure 16 Comparison of measured and calculated delamination lengths and widths (see Table 1)

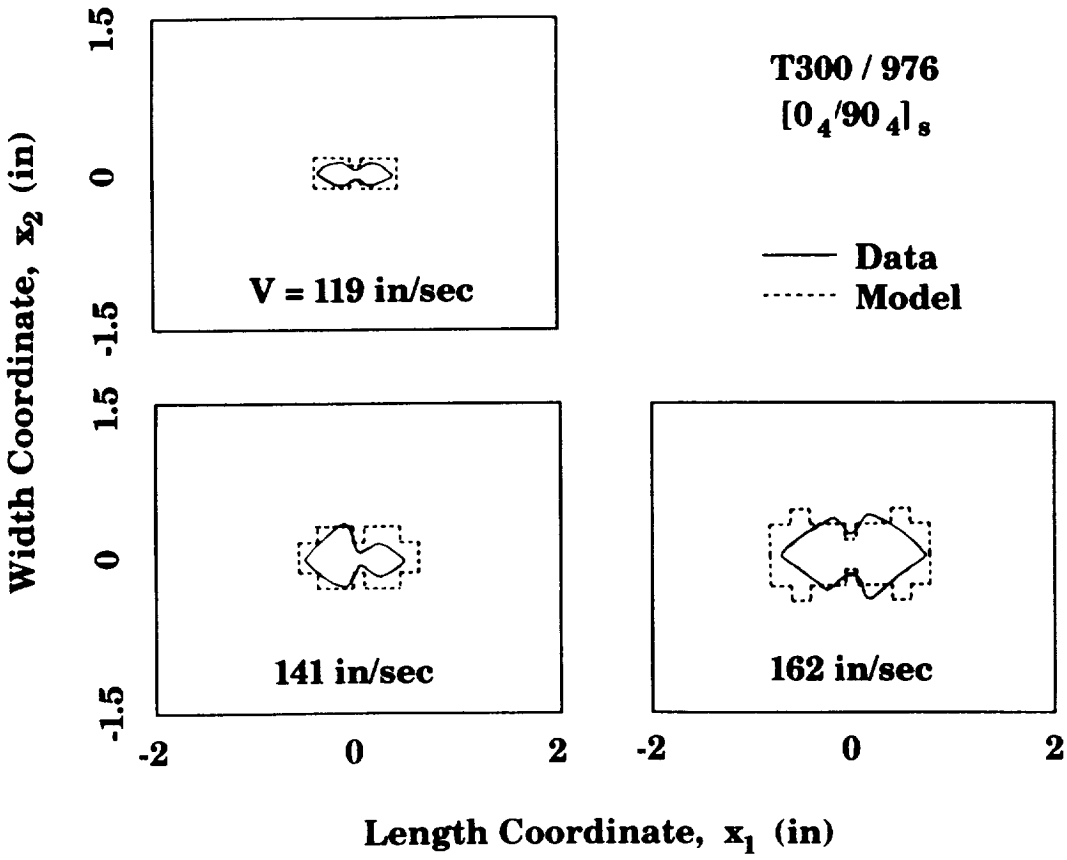

Figure 17 Comparison of measured and calculated delamination shapes at three different velocities (impactor mass m = 0.355 lbm)

CONCLUDING REMARKS

The results presented in this paper show that the model and the corresponding computer code IMPACT-ST can be used to calculate the sizes, shapes, and locations of delaminations in plates subjected to transverse, non-penetrating impact of a solid object. Hence, the computer code should be useful as an engineering design tool.

REFERENCES

1. Clark, G. "Modelling of Impact Damage in Composite Laminates," Composites, Vol. 20 (1989), pp. 209-214.

2. Bostaph, G.M. and W. Elber. "A Fracture Mechanics Analysis for Delamination Growth During Impact on Composite Plates," *Advances in Aerospace Structures, Materials, and Dynamics*, American Society of Mechanical Engineers, New York, 1983, pp. 133-138.

3. Grady, J.E. and C.T. Sun. "Dynamic Delamination Crack Propagation in a Graphite/Epoxy Laminate," *Composite Materials: Fatigue and Fracture*, ASTM STP 907, H. T. Hahn (ed.), American Society for Testing and Materials, Philadelphia, PA, 1986, pp. 5-31.

4. Grady, J.E. and K.J. DePaola. "Measurement of Impact-Induced Delamination Buckling in Composite Laminates," *Dynamic Failure; Proceedings of the 1987 SEM Fall Conference*, Society for Experimental Mechanics, 1987, pp. 160-168.

5. Liu, D. "Delamination in Stitched and Nonstitched Composite Plates Subjected to Low-Velocity Impact," *Proceedings of the American Society for Composites, Second Technical Conference*, American Society for Composites, 1987, pp 147-155.

6. Liu, D. "Impact Induced Delamination - A View of Bending Stiffness Mismatching," Journal of Composite Materials, Vol. 22 (1988), pp. 674-692.

7. Wu, H.T. and G.S. Springer. "Impact Induced Stresses, Strains, and Delaminations in Composite Plates," Journal of Composite Materials, Vol. 22 (1988), pp. 533-560.

8. Gosse, J.H. and P.B.Y. Mori. "Impact Damage Characterization of Graphite/Epoxy Laminates," *Proceedings of the American Society for Composites, 3rd Technical Conference on Composite Materials*, American Society for Composites, 1988, pp. 187-193.

9. Gosse, J.H., P.B.Y. Mori and W.B. Avery. "The Relationship Between Impact-Induced Stress States and Damage Initiation and Growth in Composite Plates," *Materials - Processes: The Intercept Point*,Society for the Advancement of Materials and Process Engineering, 1988, pp. 187-193.

10. Chang, F.K., H.Y. Choi and S.T. Jeng. "Characterization of Impact Damage in Laminated Composites," *Tomorrow's Materials: Today, 34th International SAMPE Symposium and Exhibition*, Zakrzewski, et al (ed.), Society for the Advancement of Materials and Process Engineering, 1989, pp. 702-713.

11. Joshi, S.P. and C.T. Sun. "Impact Induced Fracture in a Laminated Composite," Journal of Composite Materials, Vol. 19 (1985), pp. 51-

66.

12. Guynn, E.G. and T.K. O'Brien. "The Influence of Layup and Thickness on Composite Impact Damage and Compression Strength," *26th AIAA/ASME/ASCE/AHS Structures, Structural Dynamics and Materials Conference*, 1985, pp. 187-196.

13. Sun, C.T. and M.G. Manoharan. "Growth of Delamination Cracks Due to Bending in a $[90_5/0_5/90_5]$ Laminate," Composites Science and Technology, Vol. 34 (1989), pp.365-377.

14. Salpekar, S.A. and T.K. O'Brien. "Combined Effects of Matrix Cracking and Stress-Free Edges on Delamination," NASA TM-102591, 1990.

15. O'Brien, T.K. "Analysis of Local Delaminations and Their Influence on Composite Laminate Behavior," *Delamination and Debonding of Materials*, ASTM STP 876, W. S. Johnson (ed.), American Society for Testing and Materials, Philadelphia, PA, 1985, pp. 282-297.

16. O'Brien, T.K. "Towards a Damage Tolerance Philosophy for Composite Materials and Structures," *Composite Materials: Testing and Design*, ASTM STP 1059, P. A. Lagace (ed.), American Society for Testing and Materials, Philadelphia, PA, 1990.

17. Crossman, F.W. and A.S.D. Wang. "The Dependence of Transverse Cracking and Delamination on Ply Thickness in Graphite/Epoxy Laminates," *Damage in Composite Materials*, ASTM STP 775, K. L. Reifsnider (ed.), American Society for Testing and Materials, Philadelphia, PA, 1982, pp. 118-139.

18. Lessard, L. "Compression Failure in Laminated Composites Containing an Open Hole," Ph.D. Dissertation, Stanford University, Department of Aeronautics and Astronautics, 1989.

19. Broek, D. *Elementary Engineering Fracture Mechanics*, Martinus Nijhoff , The Hague, 1982.

20. Timoshenko, S.P. and J.N. Goodier. *Theory of Elasticity*, McGraw-Hill, New York, 1970.

21. Yang, S.H. and C.T. Sun. "Indentation Law for Composite Laminates," NASA CR-165460, 1981.

22. Wu, H.T. and F.K. Chang. "Transient Dynamic Analysis of Laminated Composite Plates Subjected to Transverse Impact," Computers and Structures, Vol. 31 (1989), pp. 453-466.

23. Wilson, E.L., R.L. Taylor, W.P. Doherty and J. Ghaboussi. "Incompatible Displacement Modes"," *Numerical and Computer Methods in Structural Mechanics*, S.J. Fenves, et al (ed.), Academic Press, New York, 1973, pp. 43-57.

24. Taylor, R.L., P.J. Beresford and E.L. Wilson. "A Non-Conforming Element for Stress Analysis," International Journal for Numerical Methods in Engineering, Vol. 10 (1976), pp. 1211-1219.

25. Sjoblom, P.O., J.T. Hartness and T.M. Cordell. "On Low-Velocity Impact Testing of Composite Laminates," Journal of Composite Materials, Vol. 22 (1988), pp. 30-52.

26. Finn, S.R. "Delaminations in Composite Plates Under Transverse Static or Impact Loads," Ph.D. Dissertation, Stanford University, Department of Aeronautics and Astronautics, 1990.